Journal of Applied Polymer Science

Morphology Development, Melt Linear Viscoelastic Properties and Crystallinity of Polylactide/Polyethylene/Organoclay Blend Nanocomposites

Mehdi Haji Abdolrasouli,[1] Hossein Nazockdast,[2] Gity Mir Mohamad Sadeghi,[2] Joachim Kaschta[3]

[1]Department of Polymer Engineering, Amirkabir University of Technology, Mahshahr, Iran

[2]Department of Polymer Engineering & Color Technology, Amirkabir University of Technology, Tehran, Iran

[3]Institute of Polymer Materials (LSP), Friedrich-Alexander-University Erlangen-Nuremberg, Erlangen, Germany

Correspondence to: H. Nazockdast (E-mail: nazdast@aut.ac.ir)

ABSTRACT: Polylactide/polyethylene blends (PLA/PE) and their nanocomposites were prepared via the melt blending process. The effects of organoclay, compatibilizer (PE-g-MA), and PE content on morphology, linear viscoelastic properties of the melt and cold crystallization of the samples have been studied. The Palierne model is applied to predict the rheological behavior of unfilled blends. It implies that there is a quantitative agreement between model and experimental data for low PE content blend. From WAXD and the rheological behavior, it is shown that organoclay exhibits a higher extent of intercalation and dispersion in PLA/PE/organoclay nanocomposite than in PLA/organoclay nanocomposite. The DSC results present that the addition of compatibilizer into blend nanocomposite increases cold crystallization temperature of PLA by about 3°C. This can be explained by the role of compatibilizer in transfer of a part of organoclay from PLA matrix to droplets resulting in increase of PLA chain mobility and, therefore, slightly greater cold crystallization temperature. © 2014 Wiley Periodicals, Inc. J. Appl. Polym. Sci. **2015**, *132*, 41300.

KEYWORDS: clay; crystallization; morphology; rheology

Received 18 May 2014; accepted 16 July 2014
DOI: 10.1002/app.41300

INTRODUCTION

In recent years, polymeric systems based on renewable resources have received significant attention from both the academic and industrial point of view due to environmental and economic issues frequently associated with petroleum-based polymers.[1] The potential of these so-called green polymers in packaging, textile and automotive applications is being explored by many researchers and industries.[2–4] Polylactide (PLA) is among the most extensively studied renewable materials. Being bio-based and bio-compostable together with several other favorable properties such as high strength, stiffness (at room temperature), and good processability have made PLA to be an excellent candidate for replacing the conventional petroleum-based polymers.[5] However, serious limitations, including brittleness, limited thermal stability during the melt processing, low heat deflection temperature, and high cost of PLA are major obstacles for commercialization in some applications.[6] A less expensive and more practical strategy to overcome these limitations and, hence, to improve other properties such as mechanical strength and crystallization behavior are blending of PLA with other polymers such as natural rubber,[7] ethylene-co-vinyl acetate,[6] polyethylene,[8] acrylonitrile-butadiene-styrene copolymer,[9] poly(epichlorohydrin-co-ethylene oxide),[10] thermoplastic polyolefin,[11] and poly(caprolactone).[12]

It is well known that the performance of an immiscible polymer blend system is not only dependent on the intrinsic characteristics of its components, but also is highly dependent on phase morphology and interfacial adhesion; both are closely related to flow histories and the viscoelasticity of the polymer components.[13] Viscosity ratio, melt elasticity of the components, shear rate, and type of flow are among the important parameters that determine the morphology in polymer blends.[14,15] Blends of PLA and PE are usually incompatible and, therefore, show coarse morphology and poor mechanical performance due to the low interfacial adhesion between PLA and PE phases. To overcome this, compatibilizers are used to reduce the interfacial tension, control the morphology and improve the interface adhesion between PLA and PE phases. Su et al. found that in blends of polylactide and linear low-density polyethylene, an ideal interfacial adhesion between the two phases was obtained via in situ compatibilization using glycidyl metacrylate-grafted poly(ethylene-octene) copolymer as a compatibilizer.[16] Anderson et al. showed that the toughening of polylactide was

Table I. Codes and Compositions of Prepared Samples in Internal Batch Mixer

Sample	Code	Composition
Virgin PLA	PLAg	100
Melt processed PLA	PLAp	100
Virgin PE	PEg	100
Melt processed PE	PEp	100
PLA/PE	PLA/PE10	90/10
PLA/PE	PLA/PE20	80/20
PLA/PE	PLA/PE30	70/30
PLA/PE/PE-g-MA	PLA/PE12/C8	80/12/8
PLA/Cloisite 30B	PLA/N4	100/4
PLA/Cloisite 30B	PLA/N5	100/5
PE/Cloisite 30B	PE/N4	100/4
PE/PE-g-MA/Cloisite 30B	PE/C8/N4	92/8/4
PLA/PE/Cloisite 30B	PLA/PE10/N4	90/10/4
PLA/PE/Cloisite 30B	PLA/PE20/N4	80/20/4
PLA/PE/Cloisite 30B	PLA/PE30/N4	70/30/4
PLA/PE/PE-g-MA/Cloisite 30B	PLA/PE12/C8/N4	80/12/8/4

achieved only when a poly (L-lactide)-polyethylene block copolymer was used as a compatibilizer in polylactide/polyethylene blends.[8] Kim et al. studied blends of polylactide and low-density polyethylene and found that the droplet size of polyethylene is reduced and the tensile properties increased significantly by using a reactive compatibilizer having glycidyl methacrylate functional group.[17]

Polymer organoclay nanocomposites have received considerable attention in both scientific and technological areas, due to their dramatically enhanced physical and mechanical properties, thermal stability, flame retardancy, and barrier properties ever at very low-filler loadings.[9,18] In the case of blend nanocomposites based on layered silicate the degree of improvement is extremely dependent on the quality of organoclay dispersion. Furthermore, the degree of intercalation and/or exfoliation is shown to have a large impact.[19,20] Generally, the extent of intercalation and/or exfoliation of the organoclay is determined by the chemical modification,[21] the concentration of organoclay,[22,23] the viscosity,[12,24] the affinity of the organoclay to the polymer matrix[25,26] as well as by processing conditions.[27] In this context, polyolefines are known to have very low affinity to organoclay and these polymers are not capable to intercalate into organoclay.[28]

It is well known that the rheological properties of multiphase systems including particulate suspensions are very sensitive to structure, size, shape, and surface characteristics of the dispersed phase. Therefore, rheology has been used as a powerful method, complementary to conventional methods such as WAXD and TEM, to study structure of polymer clay nanocomposites. Moreover, the rheological studies provide valuable information about the processability of these materials in the melt processing.[29]

The main objective of this work is to study the phase morphology and melt linear viscoelastic properties of Polylactide/Polyethylene/organoclay blend nanocomposites. It is attempted to determine the extent of intercalation of organoclay and its localization in Polylactide/Polyethylene blend by means of linear viscoelastic measurements in the melt state. In addition the nonisothermal cold crystallization behavior is investigated, with the further objective of relating filler localization and macroscopic properties.

EXPERIMENTAL

Materials

A Polylactide (PLA), NatureWorks 3001D commercialized by Cargill-Dow with a melt flow rate of 22 g/10 min (210°C at 2.16 kg) was used as matrix. It contains 92% L-lactide and 8% meso-lactide. The latter isomer is added to the L-lactide to limit crystallinity and, hence, promote higher toughness.[30] The minor phase was a linear low density polyethylene co-polymer (PE) with butane as co-monomer and melt flow rate of 2.2 g/10 min (190°C at 2.16 kg) supplied by Tabriz Petrochemical Company under the brand name "PE0220KJ". Maleic anhydride grafted polyethylene (PE-g-MA) with melt flow rate of 2 g/10 min (Fusabond E100 supplied by DuPont Co.) was used as compatibilizer. An organophilic methyl, tallow, bis-2-hydroxyethyl, quaternary ammonium exchanged montmorillonite (MT2EtOH Cloisite 30B supplied by Southern Products Co.) was used as organoclay filler.

Sample Preparation

Polymer blends and polymer blend nanocomposites varying in blend ratio as listed in Table I were prepared. The organoclay concentration was set to 4 parts per 100 part of polymers (4 phr) and the weight ratio of compatibilizer (PE-g-MA) to organoclay was 8/4 for all the samples unless otherwise specified. All samples were prepared by feeding all components at the same time into a 60 cm^3 laboratory internal mixer laboratory (Brabender Plasticorder W50) at temperature 180°C, at a rotor speed 60 rpm and a residence time of 8 min. Before mixing, PLA and PE-g-MA polymers and the organoclay were dried in an oven at 80°C for 24 hr. All the samples were cooled in air at room temperature after blending.

Characterization Methods

WAXD experiments were performed using a Phillips X'pert diffractometer with Cu-Kα radiation of wavelength (λ) = 0.154 nm, generated at 40 kV, and 40 mA. The diffractograms were scanned at ambient temperature in the 2θ range from 1.5° to 10°. Measurements were recorded every 0.02°.

The morphology of the blends was studied using a scanning electron microscope, FE-SEM, (PHILIPS XL30, Netherlands) operated at 20 kV accelerating voltage. The samples were cryogenically fractured after a storage time in liquid nitrogen of 15 min. The fracture surfaces were coated with gold for enhanced conductivity using a sputter coater.

A TEM, Philips CM-200 operated at 200 kV, was used to study the state of organoclay dispersion in the nanocomposite samples. TEM samples were prepared by using cryo-microtoming at −80°C.

The linear viscoelastic behavior of the samples in the melt was studied by using a rheometric mechanical spectrometer, RMS,

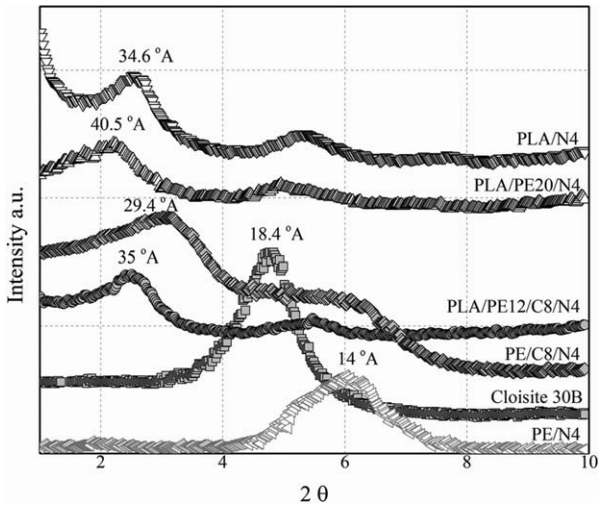

Figure 1. WAXD patterns of Cloisite 30B, uncompatibilized PE/organoclay, compatibilized PE/organoclay, PLA/organoclay, uncompatibilized PLA/PE/organoclay, and compatibilized PLA/PE/organoclay nanocomposites.

(Paar Physica UDS 200). All the measurements were conducted at 180°C in parallel plate fixture with diameter equal to 25 mm and 1 mm gap. The linear viscoelastic region was determined by monitoring storage modulus in a dynamic strain amplitude sweep experiment.

Nonisothermal crystallization behavior of the samples was determined using a NETZSCH DSC-200F3 differential scanning calorimeter. In the nonisothermal cold crystallization process, the samples were first heated from room temperature to 180°C at a rate of 10°C/min, then held at 180°C for 5 min to eliminate the thermal history. Then, the samples were quenched to room temperature at a rate of 60°C/min and heated to 180°C at a rate of 3°C/min.

RESULTS AND DISCUTION

Morphological Characterization

WAXD Results. Figure 1 shows the WAXD patterns of organically modified montmorillonite (Cloisite 30B) and the prepared nanocomposite samples. The interlayer d-spacing of the nanocomposites, calculated based on Bragg's formula, are also shown in this figure. The organoclay exhibits one characteristic peak at $2\theta = 4.83°$ which corresponds to the interlayer d-spacing of the modified layers of montmorillonite (18.4°A).

These results indicate that PE is not capable of increasing the interlayer d-spacing of the organoclay (Cloisite 30B). A collapsed structure with lower d-spacing is obtained as a result of alkyl ammonium modifier degradation. However, for compatibilized PE/organoclay sample (PE/C8/N4) the main characteristic peak of the organoclay shifts from $2\theta = 4.83°$ to lower angle ($2\theta = 3.00°$) that suggests an increase in interlayer d-spacing of the organoclay platelets as a result of enhancing effect of compatibilizer (PE-g-MA) in increasing extent of melt intercalation of organoclay.

As it can be seen in this figure, the main characteristic peak of organoclay in PLA/organoclay sample (PLA/N4) shifts to lower angles indicating the great potential of PLA for improvement of the intercalating of organoclay. The great affinity of PLA to Cloisite 30B originates from hydrogen bonds formed between the carbonyl groups of PLA and the hydroxyl ethyl groups (–CH2–CH2OH) on the surface of Cloisite 30B. Therefore, PLA molecules can easily maintain contact with the surface of the organoclay and penetrate into the silicate galleries.

Comparing the WAXD patterns of PLA/N4 and PE/C8/N4 samples reveals to a much greater extent the melt intercalation in PLA/organoclay compared to compatibilized PE/organoclay.

From these results, one may conclude that the presence of PE in the uncompatibilized blend with organoclay (PLA/PE20/N4) causes a shift in main characteristic peak of organoclay to lower angle in comparison with PLA/organoclay nanocomposite (PLA/N4). Adding PE to PLA increases the blend's viscosity (see Figure 5) and, therefore, shear stress which is transferred to the organoclay during melt mixing leads to greater delamination of organoclay.

It is also interesting to note that, as shown in this figure, using compatibilizer (PE-g-MA) in blend nanocomposite (PLA/PE12/C8/N4) shifts the main characteristic peak of organoclay from $2\theta = 2.17°$ into $2\theta = 2.52°$ that implies reduction in the extent of organoclay intercalation in PLA/PE12/C8/N4. This may be explained in terms of transfer of a part of organoclay from PLA phase to PE phase where capability in organoclay intercalation is lower.

TEM Results. Figure 2 shows the TEM graph of the PLA/organoclay sample containing 4 phr organoclay. This sample shows an intercalated and/or partially exfoliated type structure. The highly intercalated organoclays, marked by the arrows in the image, are the reasons for the diffraction peak observed in the WAXD patterns observed of PLA/organoclay nanocomposite.

FE-SEM Results of Filled and Unfilled Blend Samples. Figure 3(a,b) shows FE-SEM micrographs of PLA/PE10/N4 and PLA/PE20/N4 blend nanocomposites containing 4 phr organoclay. Comparing these micrographs with those obtained for corresponding unfilled blends (PLA/PE10 and PLA/PE20), which are shown in Figure 4(a,b), indicates that the presence of organoclay greatly reduces the particle size of the dispersed phase. It has been suggested that incorporation of organoclay into a

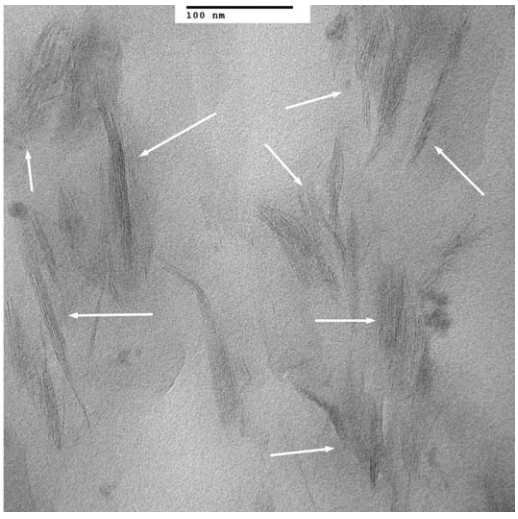

Figure 2. TEM graph of the PLA/organoclay nanocomposite (PLA/N4).

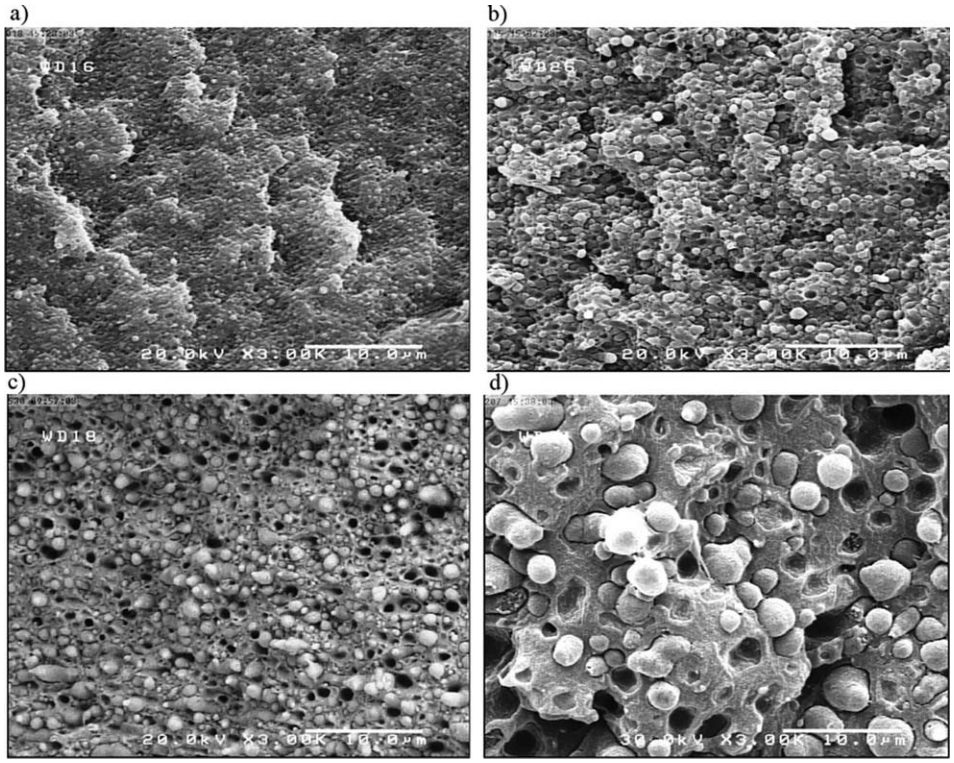

Figure 3. FE-SEM micrograph of different filled blend nanocomposites of PLA/PE/C/N: (a) 90/10/0/4, (b) 80/20/0/4, (c) 70/30/0/4, and (d) 80/12/8/4.

polymer blend sample can reduce the droplet size by three different mechanisms, (a) changes of the viscosity of the phases due to the nonuniform distribution of the organoclay, (b) compatibilization by elevated concentrations of organoclay at the interface, and (c) reduction of coalescence by the presence of a solid barrier around the polymer droplets of the minor phases.[31,32]

To investigate the role of viscosity changes on the observed morphology, dynamic viscosity curves of the melt processed PLA (PLAp), PLA nanocomposite (PLA/N4), PE nanocomposite (PE/N4), and melt processed PE(PEp) are shown in Figure 5. It can be seen that while the incorporation of organoclay into PLA results in a decrease of melt viscosity, it has no effect on melt viscosity of PE in the frequencies above 10 rad/s which is in the range of frequency estimated the shear rate is induced by the mixer (at processing temperature of 180°C). Therefore, owing to the fact that PE is the more viscous phase, the decrease in melt viscosity of PLA/organoclay phase cannot contribute to the significant reduction of average dispersed domain size of PE observed in the blend nanocomposites.

Young's equation is used to estimate the position of organoclay in blend nanocomposites by evaluating the wetting coefficient ω_a in thermodynamic equilibrium:

$$\omega_a = \frac{\gamma_{\text{organclay\_A}} - \gamma_{\text{organclay\_B}}}{\gamma_{A\_B}}, \quad (1)$$

where $\gamma_{\text{organoclay\_A}}$ and $\gamma_{\text{organoclay\_B}}$ are the interfacial tensions between the organoclay and polymer A or B, respectively, and $\gamma_{A_B}$is the interfacial tension between polymer A and B. If $\omega_a > 1$, the organoclay is located within A-phase, if $-1 < \omega_a < 1$, the organoclay concentrates at the interface, and if $\omega_a < -1$, the organoclay is selectively distributed in the B-phase. Interfacial energy between two components calculates from the surface tensions of components using the geometric mean which is valid between a low energy material and a high energy material:

$$\gamma_{12} = \gamma_1 + \gamma_2 - 2\left(\sqrt{\gamma_1^d \gamma_2^d} + \sqrt{\gamma_1^p \gamma_2^p}\right), \quad (2)$$

where γ_1, γ_2 are the surface tensions of components 1 or 2 ; γ_1^d, γ_2^d are the dispersive parts of the surface tensions of components 1 or 2, and γ_1^p, γ_2^p are the polar parts of the surface tensions of components 1 or 2, respectively.

In this work, the surface tension values of PLA,[12,33] PE,[34,35] and organoclay (Cloisite 30B)[36] summarized in Table II are obtained from the literature. Owing to the lack of high temperature data for the blend components, the values of the surface energy of PLA and PE in the molten state (180°C) are extrapolated from literature values at reference temperature using the temperature coefficient of 0.06 mJ m^{-2} for PLA and of 0.058 mJ m^{-2} for PE, respectively, assuming that the polarity is independent of temperature.

Based on the values of the surface tensions, the interfacial tensions between the pairs of components are calculated according to Eq. 2 (see Table III).

Setting PLA as polymer A and PE as polymer B the wetting coefficients calculated using Young's equation are also

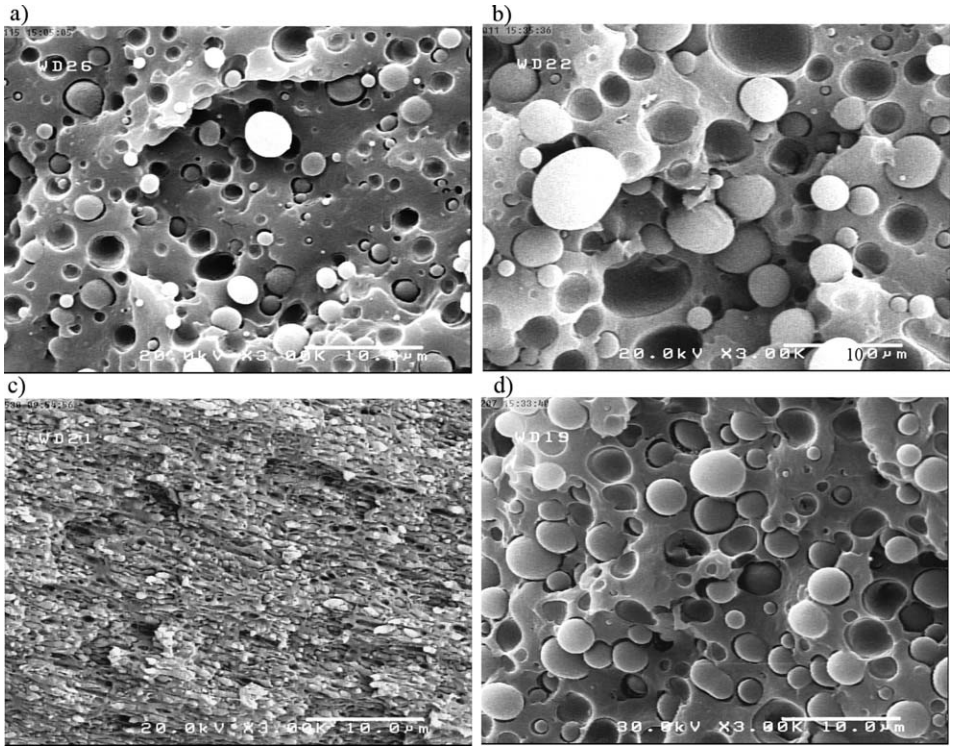

Figure 4. FE-SEM micrograph of different unfilled blends of PLA/PE/C: (a) 90/10/0, (b) 80/20/0, (c) 70/30/0, and (d) 80/12/8.

summarized in Table III. From these results, one may suggest that, at the equilibrium state, the organoclay thermodynamically tends to be located in the PLA phase ($\omega_a = 2.43$) according to the surface tension values of PLA obtained by Biresaw et al.[33] and in the interface phase ($\omega_a = 0.955$) according to the surface tension values of PLA obtained by Wu et al.[12] However, kinetically and in light of the chain mobility of polymer phases, this is closer to mind that the localization of organoclay in PLA is favored because of the lower melt viscosity of that polymer (see Figure 5). Hence, in nanocomposite samples of blend with PLA as a matrix, reduced droplet coalescence in conjunction with localization of the organoclay at the interface are the most probable mechanisms and the change of disperse/matrix viscosity ratio is less probable.

The SEM micrograph of PLA/PE30/N4 blend nanocomposite shown in Figure 3(c) suggests a spherical morphology while PLA/PE simple blend with blend ratio of 70/30 w/w shows a semicocontinuous morphology [see Figure 4(c)]. These results demonstrate that the presence of organoclay in PLA phase hinders the coalescence of PE droplets to form a continuous phase and/or stabilizes the PE droplet by reducing the interfacial tension between PLA matrix and PE dispersed phase.

Figure 3(d) shows SEM micrograph of compatibilized blend with organoclay (PLA/PE12/C8/N4). As it can be seen, the PE particles size in this sample is larger than that of uncompatibilized blend with organoclay (PLA/PE20/N4). This may be attributed to the reduction of the coalescence process due to the decrease of organoclay concentration in the PLA phase and the localization of a part of organoclay in the dispersed phase.

From Figure 4(d) one may notice that average volume diameter of particles in uncompatibilized PLA/PE blend (PLA/PE20) is reduced from 5.4 to 3.09 μm in compatibilized PLA/PE blend containing 8 wt % of PE-g-MA (PLA/PE12/C8). It indicates that the addition of a compatibilizer (PE-g-MA) reduces the

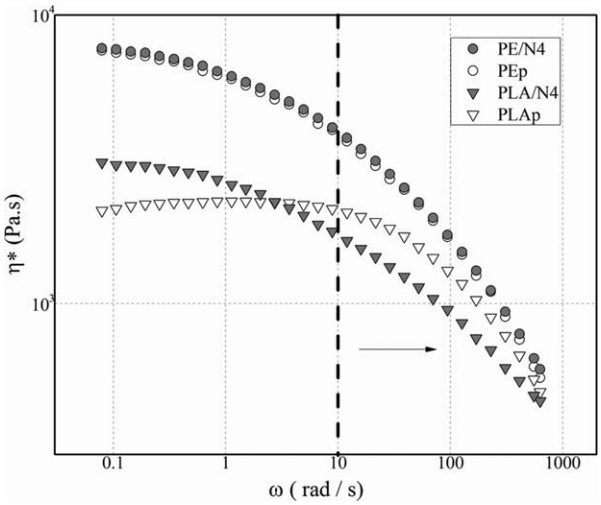

Figure 5. Complex viscosity as a function of frequency for melt processed PLA, melt processed PE, PLA/organoclay and PE/organoclay nanocomposites.

Table II. Surface Tensions and Temperature Coefficients for PLA, PE, and Cloisite 30B

Material	Total surface energy (mJ m^{-2})	Dispersive surface energy (γ^d mJ m^{-2})	Polar surface energy (γ^p mJ m^{-2})	Temperature coefficient
PLA	33.9[a]	30[a]	3.9[a]	−0.06
	41.18[b]	13[b]	28.17[b]	
PE	26.58[c]	26.58[c]	0	−0.057
Cloisite 30B	35.0	22.4	12.6	-

[a] Extrapolated from experimental values (22°C).[33]
[b] Extrapolated from experimental values (25°C).[12]
[c] Extrapolated from experimental values (20°C).[34,35]

coalescence process through stabilizing the interface between two phases.[37]

Rheological Behavior

Frequency Sweep of Unfilled Samples. Figure 6 shows the storage modulus of unfilled PLA/PE blends for various compositions. The storage modulus of all blends reveals an excess of elasticity with regard to the PLA phase. The enhancement of elasticity of the blends when compared to pure phases, in the low frequencies, was reported by many researchers for different polymer blends.[38–41] This behavior can be attributed to changing the total area of the interface and relaxation process of dispersed phase droplets during oscillatory shear flow. When the concentration of dispersed phase (PE) increases from 10 to 20 wt %, it is observed that the diameter of dispersed phase increases [see Figure 4(b)] and in relaxation process becomes longer, leading to an increase of the storage modulus.

The blend containing 30 wt % of PE with semi co-continuous morphology [see Figure 4(c)] shows higher elasticity compared to both PLA and PE homo-polymer in the low frequencies. Generally, the contribution of the phase interface to the elasticity of the blend should be reduced with the increase in concentration, because the specific interface area is reduced after percolation of the droplet phase. Thus, it is reasonable to propose that the highest modulus of the blend containing 30 wt % of PE may be attributed to the additional elastic contribution of the co-continuous phase structure, because at that concentration level, each phase is interconnected through a continuous pathway, forming an elastic network.[42,43]

The Palierne's model has been widely used to predict quantitatively the linear viscoelastic behavior of immiscible matrix/disperse polymer blends, even at high inclusion level, taking into account droplet size, droplet polydispersity, shear,and dilatation of the interface.[44] For the simple case of an emulsion of two viscoelastic phases with uniform droplet size and constant interfacial tension, Palierne's model reduces to:[45]

$$G^*_{\text{blend}}(\omega) = G^*_m(\omega)\frac{1+3\phi H(\omega)}{1-2\phi H(\omega)}, \tag{3}$$

with $H_i(\omega)$ given by:

$$H(\omega) = \frac{4\left(\frac{\gamma}{R}\right)\left[2G^*_m+5G^*_d\right]+\left[G^*_d-G^*_m\right]\left[16G^*_m+19G^*_d\right]}{40\left(\frac{\gamma}{R}\right)\left[G^*_m+G^*_d\right]+\left[2G^*_d+3G^*_m\right]\left[16G^*_m+19G^*_d\right]}, \tag{4}$$

where γ is the interfacial tension between constituting phases, G^*_{blend}, G^*_m, and G^*_d are the complex shear modulus of the blend, polymer matrix, and dispersed phase in angular frequency ω, respectively,ϕ is the volume fraction of inclusions; R is volume-average droplet radius.

The average volume diameter of PE particles of PLA/PE10 and PLA/PE20 blend samples, measured by simple image analyzer, are found to be 2.4 and 5.4 μm, respectively.

Figure 7 compares the experimental results of shear dynamic modulus (G′, G″) as a function of frequency for unfilled PLA/PE blends, containing 10 and 20 wt % of PE, and Palierne emulsion model based on Eq. 1. The interfacial tension of 10.1 mN/m (obtained by fitting) is used to draw the figures. A quantitative agreement between experimental and predicted results is

Table III. Calculated Values of interfacial Tension and Wetting Coefficient in the Blend Nanocomposite

Sample pairs A/B	PLA/Cloisite 30B	PE/Cloisite 30B	PLA/PE
γ_{AB} (mJ m^{-2})	3.03[a]	12.77	4.00[a]
	0.33[b]	12.77	13[b]
ω_a		2.43[a]	
		0.955[b]	

[a] Based on [33].
[b] Based on [12].

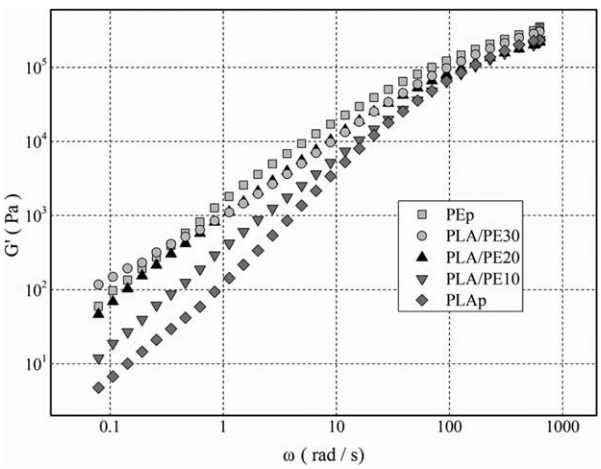

Figure 6. Storage modulus as a function of frequency for unfilled PLA/PE blends with PE content of 10, 20, and 30 wt %.

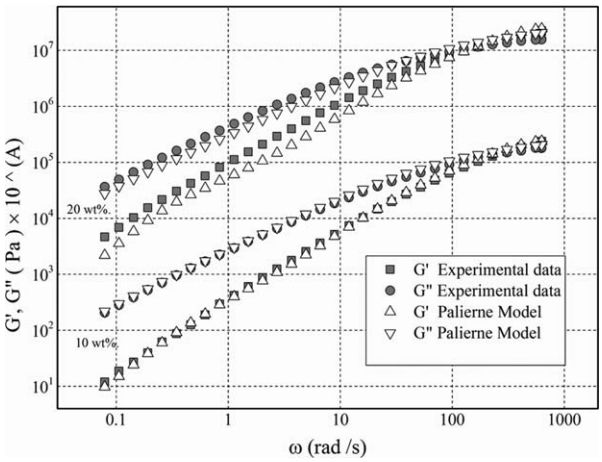

Figure 7. Comparison between storage and loss modulus of experimental data with Palierne's model with PE content of 10 and 20 wt %; PLA/PE10: A = 0; PLA/PE20: A = 2.

observed over the whole frequency range for blend prepared with PLA/PE = 90/10 while experimental data of PLA/PE containing 20 wt % of PE show positive deviation from Palierne model in the low frequencies. This deviation can be attributed to the rheological effects resulted from the small distance between PE droplets and steric interaction, which is not considered in Palierne's model.[40]

These results also show that the interfacial tension predicted by the emulsion model of Palierne (10.1 mN/m) is in fair agreement with the interfacial tension calculated by Eq. 2 using the values of the surface tensions of PLA obtained by Biresaw et al.[33] (13 mN/m, refer to morphological results) and this agreement may be inferred as the validation of the Palierne's model to estimate the interfacial tension between two phases of PLA and PE. The difference in the interfacial tension values obtained from the two approaches is mainly attributed to the different theories on which they are based.[43]

Frequency Sweep of Filled Samples. Figure 8 presents the results of complex viscosity (η^*) and storage modulus (G′) as a function of frequency for melt processed PLA (PLAp) and PLA/organoclay nanocomposites containing 4 and 5 phr organoclay (PLA/N4 and PLA/N5). In the low frequencies, the storage modulus of the PLA/organoclay nanocomposites exhibits a "pseudo solid-like behavior" due to particle-particle interconnectivity of organoclay platelets and/or polymer chains confinement by the organoclay surrounding. The strong shear thinning behavior observed in PLA/organoclay nanocomposite may be attributed to increase of molecular orientation caused by organoclay.[46]

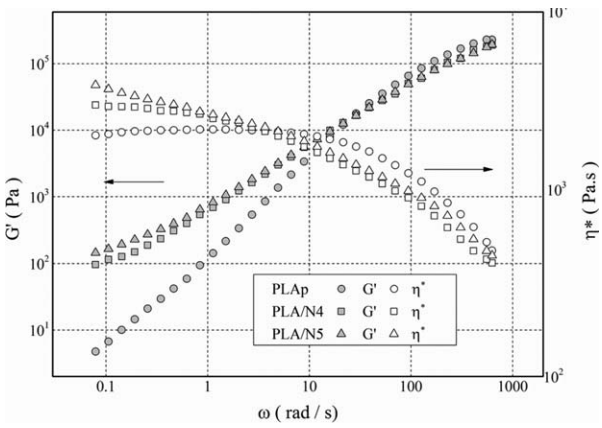

Figure 8. Complex viscosity and Storage modulus as a function of frequency for melt processed PLA and PLA/organoclay nanocomposites containing 4 and 5 phr organoclay.

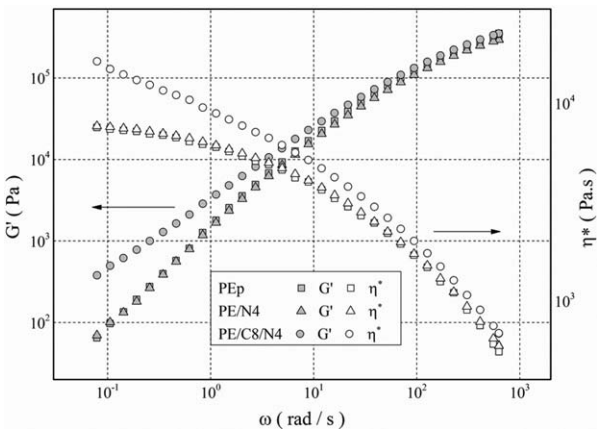

Figure 9. Complex viscosity and Storage modulus as a function of frequency for virgin PE, uncompatibilized, and compatibilized PE/organoclay nanocomposite containing 4 phr organoclay.

Figure 9 presents the results of complex viscosity (η^*) and storage modulus (G') as a function of frequency for virgin PE, uncompatibilized PE nanocomposite (PE/N4) and compatibilized PE nanocomposite (PE/C8/N4) with 4 phr organoclay. These results show that the uncompatibilized PE nanocomposite exhibits similar melt viscoelastic behavior as that of PE matrix while the compatibilized PE nanocomposites show a low frequency nonterminal behavior of storage modulus.

By comparing the results shown in Figures 8 and 9, one may notice that incorporation of 4 phr organoclay into PLA increases the storage modulus in the frequency 0.106 rad/s by about 1820% (Table IV) while incorporation of the same organoclay content into compatibilized PE leads to an increase in storage modulus by about 500% (Table IV). This suggests that

Table IV. Percentage Change in Storage Modulus of the Different Nanocomposite Samples ($\omega = 0.106$ rad/s)

Sample	Ref. sample	Percentage change in G′ (%)
PLA/N4	PLAp	1820
PLA/N5	PLAp	2700
PLA/PE10/N4	PLA/PE10	1810
PLA/PE20/N4	PLA/PE20	6400
PLA/PE30/N4	PLA/PE30	5220
PLA/PE12/C8/N4	PLA/PE20/N4	−700
PE/C8/N4	PE	500

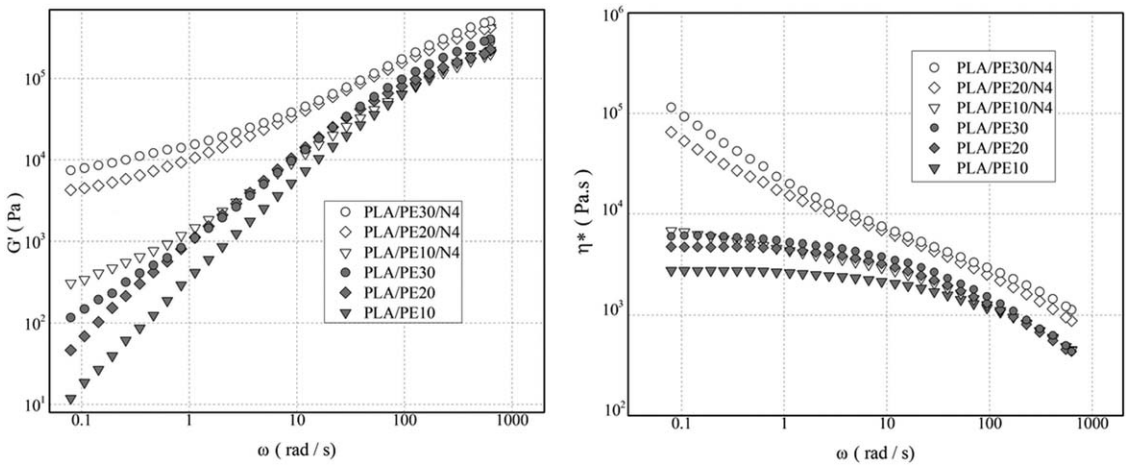

Figure 10. Comparison between frequency sweep results of unfilled and filled PLA/PE blends with different PE content.

the extent of 3D network structure formation in PLA/organoclay nanocomposite is greater than that of compatibilized PE/organoclay nanocomposite as a result of higher affinity of Cloisite 30B to PLA than to PE+PE-g-MA, which is also supported by the WAXD results.

Similar experiments performed on PLA/PE/organoclay blend nanocomposites with the same organoclay content (4 phr) but varying in PE content are shown in Figure 10. As can be noticed, these samples show much greater viscosity upturn and solid like response in the low frequencies compared to their reference samples.

Interestingly, incorporation of 4 phr organoclay has the same enhancing effect on the storage modulus of PLA and PLA/PE10 while it has a much greater effect on the solid like response of PLA/PE20 and PLA/PE30. This can be attributed to the localization of a larger part of organoclay in the PLA phase of PLA/PE20/N4 and PLA/PE30/N4(4/80 = 5 phr based on PLA phase in PLA/PE20) as a result of the higher affinity of organoclay to PLA and the lower viscosity of PLA than that of PE and, therefore, stronger 3D network formed in these samples. The extent of elasticity changes of the nanocomposites are given in Table IV for comparison. The results of storage modulus as a function of frequency obtained for PLA/N4 and PLA/N5 (Figure 8) show that extent of increase in storage modulus for PLA/N5 (about 2700%) is higher than that of PLA/N4 (by about 1800%) but is not higher than that of PLA/PE20/N4 (about 6400%) to justify that extent of increase in storage modulus and elasticity increment of PLA/PE20/N4. So this mechanism cannot be only mechanism responsible for that increase and another mechanism should be involved.

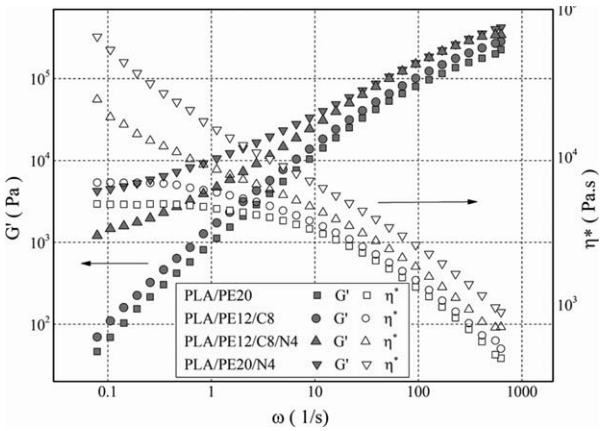

Figure 11. Complex viscosity and Storage modulus as a function of frequency for filled and unfilled blends at PLA content of 80 wt % with and without compatibilizer.

Another reason may be due to the presence of elastic PE droplets in intercalated PLA/organoclay matrix can favor break down of intercalated organoclay platelets leading to increased PLA-organoclay interface and increased probability of organoclay3D network formation. It is important to say that the lower viscosity of PLA hinders the stress transfer to organoclay tactoids effectively. In the presence of elastic PE droplets, the stress can be more effectively transferred to the tactoids. In addition, when two PE droplets move close to each other during the melt mixing process, the matrix between these droplets drains away, providing deformation field, this can also be responsible for tactoids' break down. In this case, the WAXD results support the ideas.

Figure 11 shows complex viscosity (η^*) and storage modulus (G') of PLA/PE/organoclay blend nanocomposite with and without compatibilizer (PE-g-MA) as a function of frequency. It can be seen that the addition of compatibilizer into the blend nanocomposite decreases the complex viscosity and storage modulus, in the frequency 0.106 rad/s, by about 600% and 700%, respectively. This can be attributed to the role of the compatibilizer to transfer of a part of the organoclay from PLA to PE droplets and/or to the interface resulting in a weaker 3D network structure in the matrix phase of compatibilized blend with organoclay (PLA/PE12/C8/N).

Nonisothermal Cold Crystallization Behavior. The nonisothermal cold crystallization thermograms of the samples obtained from the second heating scan are shown in Figure 12. Table V

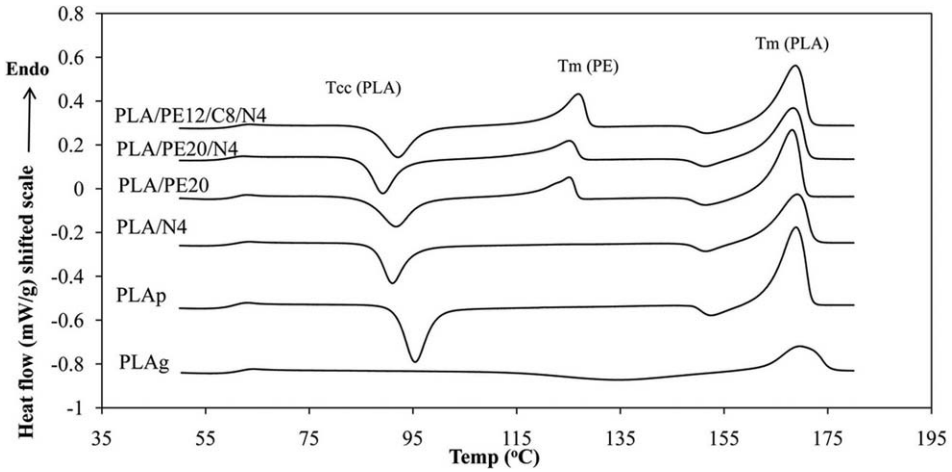

Figure 12. DSC second heating thermograms recorded for the samples at a heating rate of 3°C/min. The scans were performed directly after melt quenching.

illustrates the calorimetric parameters of the samples derived from DSC analysis. T_g is the glass transition; T_{cc} is the cold crystallization temperature peak, T_m is the melting temperature, and ΔH_c is the enthalpy of cold crystallization normalized to unit mass of PLA matrix. X_c%, the degree of cold crystallinity of the samples, is calculated by comparing ΔH_c with that for an infinitely large crystal of PLA (93.0 J/g).[47]

These results show that, while the melt processing does not have a significant effect on the glass transition and the melting temperature of PLA,[48] the T_{cc} peak of melt processed PLA (PLAp) becomes narrower and shifts to lower temperatures (from 135°C to 103.2°C). It can be also seen that melt processing increases the PLA crystallinity by about 16% (from 17% to 33%). These results suggest a greater extent of cold crystallization for melt processed PLA which can be related to a possible molecular weight reduction due to thermal degradation during melt mixing.

From these results one may notice that T_{cc} of PLA and the uncompatibilized blend (PLA/PE20) decreases with incorporation of 4 phr organoclay by about 12°C and 3°C, respectively. The drop in T_{cc} of PLA with incorporation of organoclay was also reported by Pluta et al.[49] and Wu et al.[50] This may be explained by plasticizing effect of organoclay modifier localizing in the PLA matrix and nucleating effect of organoclay.

The decreased T_{cc} leads to formation of the smaller crystallite with defect ridden lamella and less-ordered structures that can result decrease of crystallinity.[43] This can explain reduction in ΔH_c and X_c of PLA and uncompatibilized blend (PLA/PE20) with incorporation of 4 phr organoclay, as shown in Table V. Actually, the decrease of crystallinity is usually observed in the melt crystallization process of many polymer/organoclay nanocomposites which is caused by inability of polymer chains to be fully incorporated into growing crystal lamellae. In other words, the presence of high concentrations of dispersed organoclay prevents the formation of large crystalline domains because of limited space and restrictions imposed on polymer chains by a high number of platelets and/or tactoids. This leads to smaller crystallite structures and more defect crystalline lamella as well as less ordered crystals.[50–55]

These results also reveal that both cold crystallization temperature (T_{cc}) and degree of cold crystallinity (X_c) of nanocomposite based on compatibilized blend (PLA/PE12/C8/N4) is higher than that of nanocomposite based on uncompatibilized blend (PLA/PE20/N4) about 3°C and 5%, respectively. This may be

Table V. DSC Results for PLA and PLA/PE Nanocomposites[a]

Composition	T_g (°C)	T_{cc} (°C) Re-heating	T_m (°C)	ΔH_c (J/g)	X_c (%)
PLAg	61	135	169.6	16.0	17
PLAp	61.1	103.2	168.9	30.7	33
PLA/N4	60	91.1	169.1	20.8	23.3
PLA/PE20	61	91.7	125.2/168.1	21.77	29.0
PLA/PE20/N4	59.2	89.2	125.1/168.3	17.92	25.0
PLA/PE12/C8/N4	59	92.1	126.9/168.8	21.38	30.0

[a] ΔH_c and X_c are normalized to the mass of PLA.

explained by reduction of organoclay content in PLA phase of PLA/PE12/C8/N4 as a result of transfer of a part of organoclay from matrix phase (PLA) to droplet phase and/or interface due to compatibilizer addition (PE-g-MA) in accordance with results observed in WAXD and rheological results.

As shown in Figure 12 and Table V the cold crystallization temperature (T_{cc}) and degree of cold crystallinity (X_c) of PLA in PLA/PE20 blend decrease in comparison with those of melt processed PLA by about 12°C and 4%, respectively. This suggests that PE crystallized regions can affect on the crystallization of PLA because the transcrystals may generate on the surfaces of PE regions or the nucleation would occur.

CONCLUSIONS

From the melt rheology and WAXD results, it can be concluded that intercalated structures are achieved in PLA/organoclay nanocomposites while in PE/organoclay nanocomposite there is no affinity between Cloisite 30B and PE. The use of a compatibilizer (PE-g-MA) is essential to achieve intercalated structures. The linear viscoelastic measurements also demonstrate that incorporation of organoclay into PLA/PE blend with PE contents of 20 and 30 wt % dramatically increases the complex viscosity and storage modulus, in the low frequencies compared to pure PLA and PLA/PE with PE content of 10 wt %. This is attributed to the detachment of intercalated organoclay layers in the PLA matrix phase due to the stress transfer from PE particles and deformation flow field created between PE particles, leading to the formation of a stronger 3D network. It is shown that the addition of compatibilizer into blend nanocomposite decreases both complex viscosity and storage modulus, in the low frequencies, as a result of transfer of a part of organoclay from matrix phase. Considering the SEM results, it is concluded that in the presence of organoclay, more uniform and finer dispersion of the minor phase in the blend nanocomposites is obtained due to reduced coalescence of droplets and interfacial interaction enhancement. Palierne's model can predict the rheological data of unfilled PLA/PE blend with PE content of 10 wt %. Thermal analysis through DSC reveals that T_{cc} of PLA decreases with incorporation of organoclay due to plasticizing and nucleating effect of organoclay.

ACKNOWLEDGMENTS

We gratefully thank the Iran National Science Foundation INSF for the generous financial supports under grant No. 843298.

REFERENCES

1. Averous, L. *J. Macromol. Sci. Polym. Rev.* **2004**, *44*, 231.
2. Siracusa, V.; Rocculi, P.; Romani, S.; Rosa, M. D. *Trends Food. Sci. Tech.* **2008**, *19*, 634.
3. Aguilera, J. M.; Simpson, R.; Welti-Chanes, J.; Bermudez-Aguirre, D.; Barbosa-Canovas, G.; Guilbert, S.; Guillaume, C.; Gontard, N. In Food Engineering Interfaces, Springer: New York, **2011**, p 619.
4. Du, Y.; Yan, N.; Kortschot, M., A. *J. Mater. Sci.* **2014**, *49*, 2630.
5. Singh, S.; Ghosh, A. K.; Maiti, S. N.; Raha, S.; Gupta, R. K.; Bhattacharya, S. *Polym. Eng. Sci.* **2011**, *52*, 225.
6. Ma, P.; Hristova-Bogaerds, D. G.; Goossens, J. G. P.; Spoelstra, A. B.; Zhang, Y.; Lemstra, P. J. *Eur. Polym. J.* **2012**, *48*, 146.
7. Bitinis, N.; Verdejo, R.; Cassagnau, P.; Lopez-Manchado, M. A. *Mater. Chem. Phys.* **2011**, *129*, 823.
8. Anderson, K. S.; Hillmyer, M. A. *Polymer* **2004**, *45*, 8809.
9. Choe, I.-J.; Lee, J. H.; Yu, J. H.; Yoon, J.-S. *J. Appl. Polym. Sci.* **2014**, 131.
10. Zhang, K.; Ran, X.; Wang, X.; Han, C.; Han, L.; Wen, X.; Zhuang, Y.; Dong, L. *Polym. Eng. Sci.* **2011**, *51*, 2370.
11. Ho, C.-H.; Wang, C.-H.; Lin, C.-I.; Lee, Y.-D. *Polymer* **2008**, *49*, 3902.
12. Wu, D.; Lin, D.; Zhang, J.; Zhou, W.; Zhang, M.; Zhang, Y.; Wang, D.; Lin, B. *Macromol. Chem. Phys.*, **2011**, *212*, 613.
13. Utracki, L. A. Polymer Blends Handbook; Kluwer: Dordrecht, **2002**.
14. Barangi, L.; Nazockdast, H.; Taromi, F. A. *J. Appl. Polym. Sci.* **2008**, *108*, 2558.
15. Wu, D.; Zhang, J.; Zhang, M.; Zhou, W.; Lin, D. *Colloid Polym. Sci.* **2011**, *289*, 1683.
16. Su, Z.; Li, Q.; Liu, Y.; Xu, H.; Guo, W.; Wu, C. *J. Macromol. Sci. Phys.* **2009**, *48*, 823.
17. Kim, S. Y.; Shin, K. S.; Lee, S. H.; Kim, K. W.; Youn, J. R. *Fiber. Polym.* **2004**, *5*, 270.
18. Sinha Ray, S.; Okamoto, M., *Prog. Polym. Sci.* **2003**, *28*, 1539.
19. Ali, Z.; Le, H. H.; Ilisch, S.; Thurn-Albrecht, T.; Radusch, H. J. *Polymer* **2010**, *51*, 4580.
20. Abdolrasouli, M. H.; Behzadfar, E.; Nazockdast, H.; Sharif, F. *J. Appl. Polym. Sci.* **2012**, *125*, E435.
21. Pircheraghi, G.; Nazockdast, H.; Salehi, M. M. *Polym. Plast. Technol. Eng.* **2011**, *50*, 1109.
22. Risse, S.; Tighzert, L.; Berzin, F.; Vergnes, B., *J. Appl. Polym. Sci.* **2014**, *131*, 40364.
23. Khoshkava, V.; Dini, M.; Nazockdast, H. *J. Appl. Polym. Sci.* **2011**, *125*, E197.
24. Dong, Y.; Bhattacharyya, D. *Compos. A* **2008**, *39*, 1177.
25. Arroyo, M.; López-Manchado, M. A.; Valentínn, J. L.; Carretero, J., *Compos. Sci. Technol.* **2007**, *67*, 1330.
26. Marini, J.; Branciforti, M. C.; Lotti, C. *Polym. Adv. Technol.* **2009**, *21*, 408.
27. Filippi, S.; Dintcheva, N. T.; Scaffaro, R.; La Mantia, F. P.; Polacco, G.; Magagnini, P. *Polym. Eng. Sci.* **2009**, *49*, 1187.
28. Lertwimolnun, W.; Vergnes, B. *Polymer* **2005**, *46*, 3462.
29. Nazockdast, E.; Nazockdast, H.; Goharpey, F. *Polym. Eng. Sci.* **2008**, *48*, 1240.
30. Martin, O.; Avérous, L. *Polymer* **2001**, *42*, 6209.
31. Hong, J.; Kim, Y.; Ahn, K.; Lee, S.; Kim, C. *Rheol. Acta* **2007**, *46*, 469.
32. Fenouillot, F.; Cassagnau, P.; Majeste, J. C. *Polymer* **2009**, *50*, 1333.

33. Biresaw, G.; Carriere, C. J. *J. Polym. Sci. Polym. Phys.* **2001**, *39*, 920.
34. Baudouin, A.-C.; Devaux, J.; Bailly, C. *Polymer* **2010**, *51*, 1341.
35. Moreira, J. C.; Demarquette, N. R. *J. Appl. Polym. Sci.* **2001**, *82*, 1907.
36. Dharaiya, D.; Jana, S. C. *Polymer* **2005**, *46*, 10139.
37. Sundararaj, U.; Macosko, C. W. *Macromolecules* **1995**, *28*, 2647.
38. Graebling, D.; Muller, R.; Palierne, J. F. *Macromolecules* **1993**, *26*, 320.
39. Souza, A. M. C.; Demarquette, N. R. *Polymer* **2002**, *43*, 1313.
40. Huitric, J.; Mederic, P.; Moan, M.; Jarrin, J. *Polymer* **1998**, *39*, 4849.
41. Peon, J.; Vega, J. F.; Del Amo, B.; Martinez-Salazar, J. *Polymer* **2003**, *44*, 2911.
42. Omonov, T. S.; Harrats, C.; Moldenaers, P.; Groeninckx, G. *Polymer* **2007**, *48*, 5917.
43. Wu, D.; Yuan, L.; Laredo, E.; Zhang, M.; Zhou, W. *Ind. Eng. Chem. Res.* **2012**, *51*, 2290.
44. Bousmina, M. *Rheol. Acta* **1999**, *38*, 251.
45. Bousmina, M. *Rheol. Acta* **1999**, *38*, 73.
46. Pluta, M. *J. Polym. Sci. Polym. Phys.* **2006**, *44*, 3392.
47. Kalb, B.; Pennings, A. J. *Polymer* **1980**, *21*, 607.
48. Pantani, R.; De Santis, F.; Sorrentino, A.; De Maio, F.; Titomanlio, G. *Polym. Degrad. Stab.* **2010**, *95*, 1148.
49. Pluta, M.; Jeszka, J. K.; Boiteux, G. *Eur. Polym. J.* **2007**, *43*, 2819.
50. Wu, D.; Wu, L.; Xu, B.; Zhang, Y.; Zhang, M. *J. Polym. Sci. Polym. Phys.* **2007**, *45*, 1100.
51. Day, M.; Nawaby, A. V.; Liao, X. *J. Therm. Anal. Calorim.* **2006**, *86*, 623.
52. Lincoln, D. M.; Vaia, R. A.; Wang, Z. G.; Hsiao, B. S. *Polymer* **2001**, *42*, 1621.
53. Gopakumar, T. G.; Lee, J. A.; Kontopoulou, M.; Parent, J. S. *Polymer* **2002**, *43*, 5483.
54. Wu, D.; Zhou, C.; Fan, X.; Mao, D.; Bian, Z. *J. Appl. Polym. Sci.* **2006**, *99*, 3257.
55. Artzi, N.; Nir, Y.; Narkis, M.; Siegmann, A. *J. Polym. Sci. Polym. Phys.* **2002**, *40*, 1741.